

Zero-field spin splitting and spin-dependent broadening in high-mobility InSb/In_{1-x}Al_xSb asymmetric quantum well heterostructures

A. M. Gilbertson,^{1,2} W. R. Branford,¹ M. Fearn,² L. Buckle,² P. D. Buckle,² T. Ashley,² and L. F. Cohen¹

¹*Blackett Laboratory, Imperial College London, Prince Consort Road, London SW7 2BZ, United Kingdom*

²*QinetiQ, St. Andrews Road, Malvern, Worcestershire WR14 3PS, United Kingdom*

(Received 16 April 2009; revised manuscript received 3 June 2009; published 26 June 2009; corrected 26 January 2010)

We present high-field magnetotransport data from a range of 30-nm-wide InSb/InAlSb quantum wells with room-temperature mobilities in excess of $6 \text{ m}^2 \text{ V}^{-1} \text{ s}^{-1}$. Samples with the narrowest Landau level broadening exhibit beating patterns in the magnetoresistance attributed to zero-field spin splitting. Rashba parameters are extracted from a range of samples and gate biases using the difference in spin populations inferred from fast Fourier transforms of the data. The influence of Landau level broadening and spin-dependent scattering rates are investigated by magnetoconductance simulations, which provide key signatures that we were able to verify by experimental observation. These results demonstrate that in addition to the large Zeeman splitting, the combination of large and spin-dependent broadening is the significant parameter in controlling the appearance of beating in these structures.

DOI: [10.1103/PhysRevB.79.235333](https://doi.org/10.1103/PhysRevB.79.235333)

PACS number(s): 73.63.Hs, 72.20.My, 73.43.Qt, 72.80.Ey

I. INTRODUCTION

InSb has been the subject of numerous experimental and theoretical studies due to characteristic features of the bulk crystal such as a narrow band gap and light effective mass resulting in a high intrinsic electron mobility.¹ Two-dimensional electron gases (2DEGs) formed in InSb quantum wells (QWs) offer a number of advantages for device applications. Despite the difficulties associated with highly mismatched epitaxy, recent advances in the growth of high-quality InSb heterostructures on GaAs substrates have resulted in room-temperature extrinsic carrier mobilities μ reported in excess of $5 \text{ m}^2 \text{ V}^{-1} \text{ s}^{-1}$, making InSb QWs particularly attractive for high-speed electronics (high electron mobility transistors),² ballistic transport devices, and magnetic sensor applications such as nonmagnetic read heads based on extraordinary magnetoresistance.³ In the developing field of spin-based electronics, the most attractive property of InSb QWs, a large spin-orbit (SO) splitting of the conduction band, has been notoriously difficult to measure experimentally.

A large SO coupling results in a short spin lifetime, which has been measured optically to be $\tau_s \sim 0.3 \text{ ps}$ at 300 K in 20 nm InSb/InAlSb QWs (Ref. 4); however, tuning of the SO splitting via the Rashba interaction in InSb QWs, a prerequisite for most spintronic device proposals, has not been demonstrated.^{5,6} This family of devices based on the spin field effect transistor (FET) (Ref. 6) presuppose the concept that the size of the Rashba interaction, originating from the structural inversion asymmetry in the electrostatic confining potential and parameterized by the coefficient α_R , can be tuned via the application of an external electric field. Device architectures thus rely on insulated gate electrodes much like conventional FETs. Recent advances in InSb QW FET technology have demonstrated improvements in performance over Si counterparts based on equivalent device scales,⁷ making this system a promising candidate for future spintronic applications.

The two most common techniques for measuring the

strength of the SO coupling are (i) in the observation *and fitting* of quantum interference corrections in the extreme low-field magnetoconductance to weak antilocalization (WAL) theory⁸ and (ii) in the analysis of beating patterns in the low-field Shubnikov-de Haas (SdH) oscillations in the longitudinal resistivity ρ_{xx} .⁹ Although more direct, the accuracy and indeed the validity of the latter approach are somewhat controversial due to alternative explanations for the occurrence of beating¹⁰ and the influence of Zeeman splitting.¹¹

Extensive WAL experiments have been performed on InSb/GaAs (Ref. 12) and InSb/CdTe heterojunctions,¹³ providing unambiguous evidence for the presence of SO coupling in 2DEGs formed at the heterointerfaces. In contrast, only a small number of elegant but indirect measurements of the SO coupling have been made in InSb QWs and to the best of our knowledge none use beating in ρ_{xx} . This is because of the large g factor in narrow gap materials which results in the SdH oscillations being dominated by Zeeman splitting at relatively small fields (compared to wider gap systems such as InGaAs QWs),^{11,14,15} making the observation of beating patterns particularly challenging. In addition, the high mobility in InSb QWs suppresses the emergence of the WAL feature; a requirement of which is that the phase coherence time be much greater than the momentum scattering time (since WAL is a scattering-driven phenomena). Dedigama *et al.* recently reported the first observations of WAL in a (low mobility) InSb QW supporting the presence of large SO coupling.¹⁶ In an alternative approach, Khodaparast *et al.*¹⁷ extrapolated a spin splitting to zero field in an asymmetric 30 nm InSb/InAlSb QW from electron-spin-resonance measurements. Assuming the Rashba interaction to be dominant, α_R was determined to be as high as $1.3 \times 10^{-11} \text{ eV m}$. This is larger than recent theoretical calculations in InSb/InAlSb QWs estimating α_R to be in the range of $2\text{--}7 \times 10^{-12} \text{ eV m}$.¹⁸ In this work it was also demonstrated that the bulk inversion asymmetry (BIA) contribution to spin splitting can be of significant and comparable value to that of the Rashba depending on the specific details of the heterostructure. In support of this concept, Akabori *et al.*¹⁹ recently

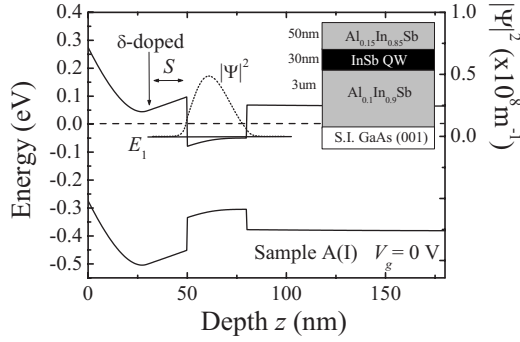


FIG. 1. Schrödinger-Poisson solution for sample A(I) at zero gate bias and 10 K in the vicinity of the QW showing the band profile (solid black line) and the single occupied ground state (dotted line) beneath the Fermi energy located at $E=0$ meV (dashed line). The position of the Te δ layer is indicated where S is the undoped spacer layer thickness. (Inset) A schematic view of the layer structure.

reported experimental results indicating that BIA was dominant in a similar narrow gap InGaSb/AlInSb QW sample. Discrepancies exist between experiment and theory of the spin splitting phenomena in narrow gap systems, and the subject would benefit from a comprehensive investigation of samples with a range of carrier densities.

Here we present high-field magnetotransport measurements on a range of single subband (gated) n -InSb/InAlSb QWs that exhibit high room- and low-temperature mobilities²⁰ with the aim of extracting information on the SO spin splitting. We previously reported on similar samples where no beating was observed in ρ_{xx} .²¹ Beating patterns in $d\rho_{xx}/dB$ and $d^2\rho_{xx}/dB^2$ are observed in the present samples only with the narrowest Landau level broadening, from which Rashba coupling parameters are directly extracted as a function of carrier density. With the use of magnetoconductance simulations, it is argued that the observation of beating effects in InSb QWs is elusive not only due to the large Zeeman splitting but also due to the combination of an inherently large, inhomogeneous, and spin-dependent broadening in these structures. The paper is organized in the following way. In Sec. II a description of the experiment and samples is given. In Sec. III the experimental results and analysis are presented. Finally, in Sec. IV some conclusions are drawn.

II. EXPERIMENT

Samples were grown by solid source molecular beam epitaxy (MBE) onto semi-insulating GaAs (001) substrates. A schematic view of the layer structure along with a typical band profile generated from a Schrödinger-Poisson model near the surface are shown in Fig. 1. In this calculation mid-gap pinning of the Fermi energy at the surface boundary was assumed. In growth order, the heterostructure consists of an accommodation layer, a 3 μm intentionally undoped $\text{In}_{0.9}\text{Al}_{0.1}\text{Sb}$ buffer layer, a 30-nm-strained InSb QW, and a 50 nm $\text{In}_{0.85}\text{Al}_{0.15}\text{Sb}$ upper barrier forming a type-I heterostructure confining both electrons and holes. The upper bar-

TABLE I. Sample parameters n_{2D} and μ at 2 and 290 K (at zero gate bias) along with nominal gate oxide thickness.

Sample	μ ($\text{m}^2 \text{V}^{-1} \text{s}^{-1}$) 2 K (290 K)	n_{2D} (m^{-2}) 2 K (290 K)	Gate oxide (nm)
Sample A(I)	27.2 (6.78)	2.32×10^{15} (3.29×10^{15})	50
Sample A(II)	26.13 (6.52)	2.51×10^{15} (3.50×10^{15})	50
Sample B(I)	39.5 (6.87)	3.28×10^{15} (4.56×10^{15})	150
Sample B(II)	39.0 (6.93)	3.21×10^{15} (4.50×10^{15})	150
Sample C	18.36 (5.07)	1.50×10^{15} (4.12×10^{15})	50

rier was δ doped with Te, separated from the QW by an undoped spacer layer of thickness $S=20$ nm. As seen in Fig. 1 the resulting QW is asymmetric both in physical barrier composition and electrostatic confining potential in the growth direction. Low-field electron transport studies in these heterostructures were recently performed, indicating that carrier mobility in these remote doped wide well structures is dominated by remote ionized impurity scattering at low temperatures.²⁰

Magnetotransport measurements were performed using conventional 40 μm wide-gated Hall bridges fabricated using optical lithography and wet etching with voltage probes separated by 200 μm . Shallow contact techniques were employed to form the Ohmic contacts and ensure that transport is via the 2D channel only. Ti/Au top gate electrodes were evaporated onto an insulating SiO_2 dielectric layer (see Table I) which covered the sample. Note that voltage probes in these devices are located sufficiently away from the current contacts so that geometric effects can be ignored.²²

The devices were measured in a cryogen-free magnet system enabling measurements to be performed over a magnetic field range of $-7.5 \text{ T} < B < 7.5 \text{ T}$ and temperatures down to 2 K. Longitudinal and Hall resistivities ρ_{xx} and ρ_{xy} were measured with magnetic field applied perpendicular to the plane of the 2DEG using a low-frequency lock-in technique at a drive current of 500 nA (the observed SdH oscillations were strongly dampened at drive currents $>1 \mu\text{A}$ due to Joule heating).

III. RESULTS AND DISCUSSION

Five samples were investigated that were fabricated from three different wafers differing only in doping density. These are labeled sample A (I and II), sample B (I and II), and sample C. To characterize the 2DEGs, the sheet carrier density n_{2D} at zero gate bias was determined both from low-field Hall effect measurements and from the SdH fundamental frequency which agreed to within 2% indicating that no parallel conduction paths are present. These values and the associated carrier mobilities, μ , are listed in Table I for each sample at 2 and 290 K. A small variation in carrier density was observed between devices from the same wafer due to the sensitivity of the 2DEGs to the presence of (spatially nonuniform) surface states at the $\text{SiO}_2/\text{InAlSb}$ interface. It is noteworthy that the samples investigated here exhibit the highest low-temperature mobilities reported in the InSb QW

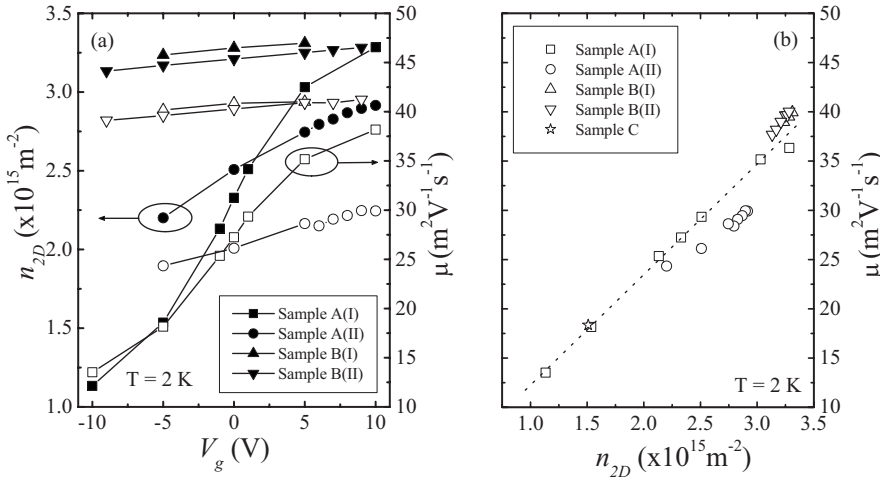


FIG. 2. (a) Sheet carrier density n_{2D} (closed symbols, left axis) and mobility μ (open symbols, right axis) for samples A(I) (squares), A(II) (circles), B(I) (upward triangle), and B(II) (downward triangle) as a function of gate bias V_g at 2 K. (b) The 2 K mobility as a function of carrier density for all samples and gate biases showing a linear relationship. The dashed line is a guide for the eyes.

system and the highest RT mobilities in all III-V QW systems reported.

Using the top gate electrode n_{2D} and μ were modulated in samples A(I), A(II), B(I), and B(II) over a range of values. Data for n_{2D} (closed symbols) and μ (open symbols) as a function of gate bias V_g obtained at 2 K are presented in Fig. 2(a). Due to difficulties in producing a high yield of low-leakage gate contacts, samples B(I) and B(II) were fabricated with a nominally thicker dielectric layer (see Table I); this is reflected in the smaller modulation of n_{2D} shown in Fig. 2(a). The gate electrode for sample C did not function at all due to excessive leakage current and so we focus our discussion on the gate dependence of the remaining four samples. As n_{2D} is increased with gate bias, μ increases steadily. This is typical for modulation-doped heterostructures whereby the increasing Fermi velocity in the 2DEG reduces the effectiveness of the Coulomb scattering from (a fixed density of) remote ionized impurities and subsequently increases the momentum scattering lifetime (related to mobility by $\tau_p = m^* \mu / e$, where m^* is the effective mass and e is the electron charge).²³ Data from all samples and gate biases are shown together in Fig. 2(b), where a general trend of increasing mobility with carrier density is evident, consistent with impurity scattering.

Figure 3(a) shows typical low-temperature recordings of the longitudinal resistivity ρ_{xx} and Hall resistance ρ_{xy} from

sample B(I) in the range of 2–20 K ($V_g = 0 \text{ V}$). At quantizing magnetic fields $\mu B \gg 1$ Landau levels (Lls) are resolved in the density of states (DoS) and plateaus emerge in the Hall resistance, quantized to values of $\rho_{xy} = h/ie^2$ (with $i = 1, 2, \dots$). The plateaus in ρ_{xy} are accompanied by minima in ρ_{xx} corresponding to when the Fermi energy lies between two Lls.

Clear single-period oscillations are observed for all samples and gate biases indicative of single subband occupation which is supported by Schrödinger-Poisson solutions of the band profiles (see Fig. 1). In Fig. 3(b) we show 2 K magnetoresistance data for samples A(II) (upper trace) and B(II) (lower trace) at 2 K where SdH oscillations are resolved at filling factors ($\nu = n_{2D} h / e B$) up to $\nu = 46$ in the higher-mobility sample as indicated by the solid arrows. Also indicated by the dotted arrows is the emergence of Zeeman splitting at odd filling factors as high as $\nu = 15$, demonstrating the presence of a large g factor. Reducing the temperature below 5 K gave no significant improvement in the resolution of the low-field SdH oscillations (not shown), indicating that at 2 K the SdH oscillations are limited by inhomogeneous LI broadening rather than thermal broadening. This is in good agreement with measurements made on similar samples down to lower temperatures (300 mK).²⁴

From the examination of Figs. 3(a) and 3(b) it can be seen that there is a distinct nonoscillatory background magnetore-

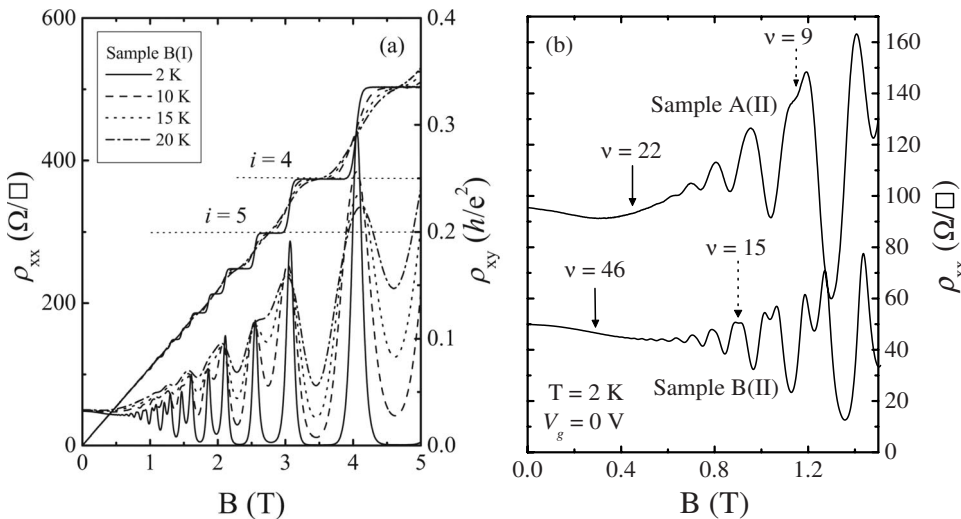


FIG. 3. (a) Longitudinal ρ_{xx} (left axis) and transverse ρ_{xy} (right axis) resistivities measured at various temperatures as a function of magnetic field B for sample B(I) ($V_g = 0 \text{ V}$) demonstrating single-period SdH oscillations and integer quantum Hall effect. (b) Low-field region of $\rho_{xx}(B)$ for samples A(II) (upper trace) and B(II) (lower trace) indicating the onset of SdH oscillations (solid arrows) and the emergence of Zeeman splitting (dotted arrows) at odd filling factors as high as $\nu = 15$.

sistance present in our samples which is temperature dependent. At low fields, ρ_{xx} contains at first negative and then a positive magnetoresistance, which becomes approximately linear at high fields. The low-field region $B < 0.4$ T depicted in Fig. 3(b) is consistent with the effects of electron-electron interactions in the presence of Zeeman spitting described by Lee and Ramakrishnan,²⁵ although, this mechanism will not be examined here. The high-field quasilinear magnetoresistance has previously been observed in InSb epilayers and is attributed to the intrinsic magnetoresistance originating from sample inhomogeneities.^{22,26}

A. Estimation of Landau level broadening

As indicated by the position of the solid arrows in Fig. 3(b), the extent of the low-field SdH oscillations of interest varies between samples. This is strongly influenced by the broadening of the Lls, Γ , and a more quantitative examination is crucial. Under the assumption that the broadening has no significant thermal contribution, a simple estimate for Γ is made from the critical field at which SdH oscillations become resolved, denoted here by B_{SdH} . Oscillations in ρ_{xx} are a manifestation of the oscillations in the DoS and so it is reasonable to assume that these will become resolved when the cyclotron energy exceeds the level broadening, then the broadening is given simply by $\Gamma = \hbar e B_{\text{SdH}} / m^*$. Due to its narrow band gap, the conduction band of InSb is highly non-parabolic and the mass becomes energy dependent. It is therefore necessary to consider these effects on m^* in estimating Γ . Within the six-band Kane model²⁷ the conduction band (near $k=0$) can be described by the dispersion relation $E(1 + E/E_g) = \hbar^2 k^2 / 2m_{cb}^*$, where E is the electron energy, k is the wave vector, E_g is the band gap, and m_{cb}^* is the effective mass at the conduction-band edge. The effective mass is related to the first derivative of the dispersion relation with respect to wave vector and is given by²⁸

$$m^*(E) = m_{cb}^* \left(1 + \frac{2E}{E_g} \right). \quad (1)$$

Since we are interested in the conduction at the Fermi energy, $E = E_F$ and using $k_F = (2\pi n_{2D})^{1/2}$ we have

$$E_F = \left(\frac{E_g^2}{4} + \frac{E_g \pi \hbar^2 n_{2D}}{m_{cb}^*} \right)^{1/2} - \frac{E_g}{2}. \quad (2)$$

This description of the effective mass agrees well with experimental data of m^* obtained from the temperature dependence of SdH oscillations in similar InSb QWs.²⁹ Using Eqs. (1) and (2) with the parameters $m_{cb}^* = 0.014m_0$ and $E_g = 0.255$ eV (taking into account the effect of strain on the band gap),¹ we calculate appropriate values for m^* which are then used in the estimation of Γ . Careful examination of both first and second derivatives of $\rho_{xx}(B)$ versus $1/B$ was required in order to determine B_{SdH} . The results of this analysis for each sample at each gate bias measured are plotted against carrier density in Fig. 4.

A relationship between Γ and n_{2D} is found such that data from different samples appear to fall close to a single line. It should be emphasized that although this simple approach has

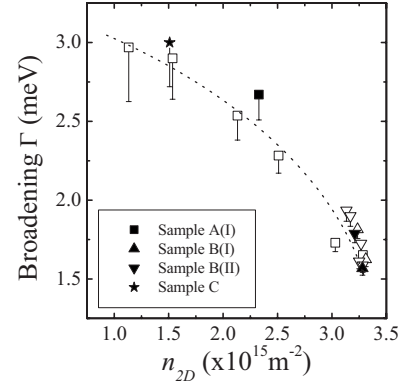


FIG. 4. Landau level broadening parameter Γ samples as a function of carrier density (including each gate bias) determined from the critical field B_{SdH} . Closed symbols represent data at zero gate bias. The dashed line is a guide for the eyes.

the advantage that it makes no assumptions of the scattering potential, in practice it is limited by the signal-to-noise ratio of the experiment which in turn limits the accuracy in determining B_{SdH} and Γ . This technique thus provides an upper limit for Γ as indicated by the error bars in Fig. 4. In sample A(II) the signal-to-noise ratio in the raw data was significantly lower than that in the other samples (which we speculate is related to $\text{SiO}_2/\text{InAlSb}$ interface effects); consequently because these data have large error bars, we have not included it in the figure.

The magnitude of Γ for the samples shown in Fig. 4 ranges from 1.5 to 3 meV. This is surprisingly large compared to the typical values extracted from GaAs/AlGaAs and InAs/GaSb systems of $\Gamma \sim 0.26$ meV (Ref. 30) and $\Gamma \sim 0.4\text{--}1.5$ meV (Refs. 31 and 32), respectively. The effect of the level broadening on the extraction of the spin splitting is discussed later in this section. It is somewhat counterintuitive that Γ is large and yet the mobility μ is high, suggesting that the scattering processes that influence Γ do not adversely effect μ . The nature of the broadening depends strongly on the range of the scattering potentials involved.³³ Since these structures have been shown to be limited by remote ionized impurities at low temperatures, it is not unreasonable to suggest that the large broadening in these samples results from the long-range nature of the scattering potential associated with remote doping. In this regime, Γ is susceptible to and determined by inhomogeneities in the local potential energy felt by the carriers. Such inhomogeneities may result from spatial variations in well width and/or interface roughness in the sample²⁰ and perhaps reflects the difficulty in the growth of high-quality InSb heterostructures on highly mismatched GaAs substrates. However, it is interesting to note that estimating Γ from data taken from a similar InSb QW sample¹⁷ grown from a different MBE source appears to show similar levels of broadening to those found here. We point out that this conjecture is clearly not universal for remote doped heterostructures, e.g., a narrow broadening of ~ 0.6 meV was found in a similar narrow gap InGaSb/AlInSb structure with a large 50 nm spacer layer in Ref. 19. In this case the mobility was relatively small compared to samples studied here and it is plausible that alloy scattering (short range) in the

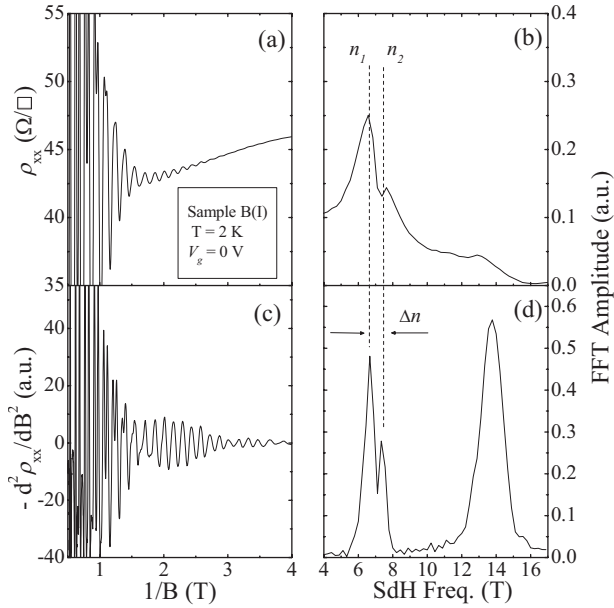


FIG. 5. (a) Low-field region of ρ_{xx} plotted against inverse field $1/B$ for sample B(I) at $V_g=0$ V and $T=2$ K. (b) Corresponding FFT spectrum of the ρ_{xx} data in (a). (c) Second derivative of the same data from sample B(I) shown in (a) resolving a clear beating pattern. (d) FFT spectrum of data in (c).

InGaSb channel in their sample may have influenced the transport.

B. Spin splitting analysis

Various authors have reported beating in the low-field SdH oscillations in the InAs (Refs. 32, 34, and 35) and InGaAs (Refs. 9, 14, 36, and 37) systems which is assigned to SO splitting of the conduction band. Beating patterns arise from the participation of two sets of SdH oscillations with similar amplitudes differing slightly in frequency analogous to optical beating. This corresponds to the presence of two types of carriers with similar densities and effective masses and is thus attributed to the spin splitting of the ground state rather than the occupation of two 2D subbands. This phenomenon allows for extraction of the total spin splitting or if dominant, the Rashba coefficient α_R from either the field dependence of the beat node positions⁹ (if more than three nodes are observed) or from the difference in carrier densities of the two spin populations $\Delta n = n_1 - n_2$ determined from a fast Fourier transform (FFT) of the low-field ρ_{xx} data.¹¹ The observation of beating patterns in InSb QWs has not been made to date.

Measurements from all samples at each gate bias show no discernible beating in the low-field ρ_{xx} data consistent with previous reports in InSb QWs. This can be seen in the data of Fig. 3(b) for samples A(II) and B(II) and Fig. 5(a) for B(I). However, careful inspection of the first and second derivative of the ρ_{xx} data with respect to B reveals a weak modulation in the SdH oscillation amplitude, far from the onset of resolved Zeeman splitting. This is demonstrated in Fig. 5(c) which shows the beating pattern in $d^2\rho_{xx}/dB^2$ of the same data in Fig. 5(a) plotted against inverse field (data have been

smoothed by a three-point adjacent averaging).

This weak beating is exhibited for all gate biases in samples B(I) and B(II) but only for $V_g=10$ V in sample A(I). Beating is not observed in sample A(II) or C. This result can be related to the level broadening and is discussed in a later next section.

The corresponding Fourier spectra of the data in Figs. 5(a) and 5(c) are shown in Figs. 5(b) and 5(d), respectively, which exhibit a clear double-peaked structure. The resolution of this structure is enhanced when performing the FFT on higher-order derivatives. Note that in order to resolve the structure from ρ_{xx} data, a field window must be chosen that excludes Zeeman split oscillations. Resolving the structure from the $d^2\rho_{xx}/dB^2$ data is less susceptible to the inclusion of Zeeman split oscillations. This can be seen in the data of Fig. 5(d), which exhibits the double-peak structure even in the presence of a significant peak at the Zeeman split (double) frequency. The carrier densities associated with each peak n_1 and n_2 can be extracted according to $n_{1,2} = f_{1,2}e/h$ [see Fig. 5(d)]. Here $f_{1,2}$ is the FFT frequency (in T) of the two peaks 1 and 2 (at this point the assignment of spin cannot be made). An asymmetry in the peak amplitudes is observed in all cases and is discussed in a later section. The sum of the two densities n_1 and n_2 matches well the total carrier density n_{2D} obtained from the low field Hall, providing strong evidence that the two SdH series originate from spin split subbands. The relatively poor resolution of the FFT spectra (due to the small number of oscillations in these low density samples) introduces uncertainties in the peak positions $f_{1,2}$ corresponding to an error in the densities of $\delta n_{1,2} \sim \pm 3 \times 10^{13} \text{ m}^{-2}$. These errors are taken into account in the determination of Δn .

It is important to rule out erroneous identifications of zero-field spin splitting simply from the observation of beating. Beating patterns can result from inhomogeneous carrier density, e.g., this can arise in experiments utilizing photoinduced carriers as demonstrated by Brosig *et al.*³¹ In our case, all measurements were performed in the dark, and since the length scale of the device is small $< 200 \mu\text{m}$, we exclude the origin of beating from this effect. It was also shown by Rowe *et al.*¹⁰ in the InAs/GaSb system that beating patterns can arise from the mixing of the SdH series from the ground-state subband and a magnetointersubband (MIS) series, which is unrelated to zero-field spin splitting. MIS scattering only occurs when the second subband becomes occupied. In our samples, no evidence for second subband occupation is found in either the FFT spectra or the gate dependence of the carrier mobility and which is supported by self-consistent band profile calculations (see Fig. 1). Therefore, in the following analysis we attribute the observed beating to the spin splitting phenomena.

Estimates of the SO coupling parameters in our material system were made using self-consistent band-structure calculations derived from the $\mathbf{k} \cdot \mathbf{p}$ method.¹⁸ While the strengths of the k -linear (β) and k -cubic (γ) Dresselhaus couplings are high in these wide well structures ($\beta \sim 3 \times 10^{-12} \text{ eV m}$ and $\gamma \sim 430 \text{ eV \AA}^3$ at $3 \times 10^{15} \text{ m}^{-2}$) and contribute significantly to the spin splitting at low densities where the Rashba effect is suppressed, their significance rapidly decreases with carrier density as the Rashba interaction is enhanced due to

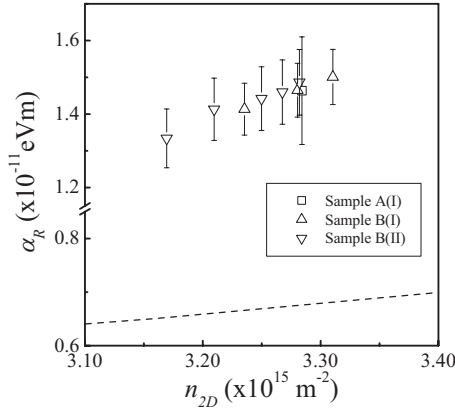


FIG. 6. Values for the Rashba coefficient α_R obtained from experimentally extracted difference in spin populations Δn as a function of carrier density n_{2D} for samples A(I), B(I), and B(II). Error bars originate from the uncertainty in FFT peak positions. The dashed line represents the calculated values of α_R from Ref. 18.

increasing electrostatic asymmetry across the QW.¹⁸ At higher carrier densities where beating is observed in our samples, the Rashba effect can be assumed to be the dominant mechanism.

With only one or two beat nodes distinguishable in our data, the Rashba parameter is determined from the difference in the spin populations (from the FFT spectra) following the approach of Engels *et al.* using¹¹

$$\alpha_R = \frac{\Delta n \hbar^2}{m^*} \sqrt{\frac{\pi}{2(n_{2D} - \Delta n)}}. \quad (3)$$

Equation (3) is derived from the parabolic energy dispersion in the presence of Rashba splitting³⁸ which leads to a spin-dependent DoS in zero field. It can be shown that incorporating the effects of band nonparabolicity analytically in the derivation of Eq. (3) yields the same result. The results of this analysis are presented in Fig. 6 as a function of carrier density.

The extracted Rashba parameter from samples B(I) and B(II) increases monotonically with carrier density. This dependence is in contrast to the results of Nitta *et al.*,¹⁴ Engels *et al.*,¹¹ Schapers *et al.*,³⁷ and Hu *et al.*³⁹ obtained in the InGaAs system who reported values of α_R which decreased with carrier density. It is noteworthy that the results in these works were obtained from top (front) gated structures where the doping layer is positioned *below the QW*. Both these dependences are fully accounted for by theoretical treatments that take into account finite barriers.^{18,40} It is established that the Rashba parameter is determined predominantly by the difference of the electron probability density function at the upper and lower QW interfaces, such that

$$\alpha_R \propto \langle E_z \rangle + [A\psi_{UI}^2 - B\psi_{LI}^2], \quad (4)$$

where the first term $\langle E_z \rangle$ represents the electric field averaged over the ground-state wave function and the second term represents the difference in the probability density functions at the upper Ψ_{UI}^2 and lower Ψ_{LI}^2 interfaces weighted by coefficients A and B containing the material parameters and

band offsets.⁴⁰ As shown in Fig. 1, the ground-state wave function in our asymmetric structures doped above the QW is weighted toward the upper interface. The application of positive gate bias lowers the potential at the left hand boundary ($z=0$) having the twofold effect of increasing the electric field across the QW [first term in Eq. (4)] and skewing the wave function further toward the upper interface [second term in Eq. (4)], which increases the Rashba parameter and accounts for the trend observed in our samples. In structures doped below the QW, the direction of the electric field is reversed, so that the opposite dependence of the Rashba parameter on carrier density is observed. This concept is consolidated by the results of Grundler, who, with the independent use of both a top and back gate, observed both dependencies of α_R on n_{2D} in an InAs 2DEG doped below the QW (Ref. 35) (using a back gate on a sample doped below the QW is equivalent to our experiment).

A second feature of Fig. 6 is that data from all three samples appear to lie on a common line. This trend is in agreement with calculations of the SO parameters in these structures¹⁸ whereby in varying the electrostatic potential in the heterostructure via the doping density and spacer thickness (or indeed gate bias), the common variable is the carrier density and data fall onto a single curve.

We can make some comments on the magnitude of α_R extracted from our samples. Due to the reduced density of states in the InSb system and the requirement of single subband occupation in these wide QWs, the carrier density in our samples is significantly lower than most previous studies of spin splitting from beating in InAs and InGaAs QWs, limiting direct comparison to just a few cases. Our extracted values of α_R agrees well with that of Khodaparest *et al.*¹⁷ obtained from a similar InSb QW—both of which are larger than those extracted from wider gap materials at comparable densities, e.g., Guzenko *et al.* studied the spin splitting in a low-doped InGaAs/InP QW (Ref. 36) and Holmes *et al.* in an InGaAs/InAlAs QW (Ref. 15) finding $\alpha_R \sim 6.5 \times 10^{-12}$ eV m ($n_{2D} \sim 3 \times 10^{15}$ m⁻²) and $\alpha_R \sim 9 \times 10^{-12}$ eV m ($n_{2D} \sim 2 \times 10^{15}$ m⁻²), respectively, from the analysis of beating. These values are consistent with the trend in the literature and the expectation that the Rashba parameter scales inversely with the band gap.⁴¹

Our experimental values are larger than theoretical calculations of α_R in these heterostructures which is indicated by the dashed curve in Fig. 6 (Ref. 18) (there are no free parameters in these calculations). One can also see that the dependence of α_R on n_{2D} is also stronger than calculation predicts which is particularly attractive for spintronic applications. We note that the expression used in Eq. (3) has the disadvantage of being derived from the DoS in zero magnetic field, while values of Δn used to calculate α_R are obtained from measurements in nonzero fields. Consequently, the contribution from the Zeeman splitting is neglected along with the field dependence of α_R and this method should be considered an estimate (particularly in narrow gap systems where g^* is large). Furthermore, Δn , which reflects the polarization of the system, changes continuously with field. Ideally, the narrowest (low) field window would be one where there are sufficient oscillations to extract the two densities. Inevitably this condition requires high-density

samples. Discrepancies between theory and experiment may also result from the presence of many-body effects such as the exchange interaction⁴² which enhance the spin splitting and are not included in the model. This may also be significant following a recent report of large exchange enhancement of the g factor in these QW structures.²⁹

C. Influence of level broadening on beating patterns

We speculate that the absence of beating in samples A(II), C, and A(I) (for $V_g < 10$ V) can be attributed to the combination of *large broadening* Γ and a large Zeeman splitting which limits the field range $B_{\text{SDH}} < B < B_Z$ over which the effects of SO splitting are observable. Here B_Z is the field at which Zeeman splitting is resolved, i.e., for $B > B_Z$ spin splitting in the 2DEG is dominated by the Zeeman effect.⁴³ The number of oscillations within this field range depends on both Γ and the carrier density n_{2D} and from this assertion it follows that only in samples with the greatest number of oscillations are the effects of beating detectable (see Fig. 4).

This conjecture may be quantified by simulations of the SdH oscillations in the presence of Rashba SO splitting. In this analysis, we consider the Landau level energy spectrum in the presence of Rashba splitting $E_{n\pm}$ for spin up (+) and spin down (-) (Ref. 44),

$$E_{n\pm} = \hbar\omega_c \left(n + \frac{1}{2} \pm \frac{1}{2} \right) \mp \frac{1}{2} (\hbar\omega_c - g^* \mu_B B) \times \sqrt{1 + \frac{8\alpha_R^2}{(\hbar\omega_c - g^* \mu_B B)^2} \frac{eB}{\hbar} \left(n + \frac{1}{2} \pm \frac{1}{2} \right)}, \quad (5)$$

where $n=1, 2, \dots$ is the Landau level index and $\omega_c = eB/m^*$ is the cyclotron frequency. Following the result of Gerhardtts *et al.*⁴⁵ the DoS takes on the Gaussian form and the magnetoconductance at $T=0$ K can be given by

$$\sigma_{xx}(B) = \frac{e^2}{2\pi\hbar} \sum_{n\pm} (n + 1/2) \exp\left(-\frac{(E_F - E_{n\pm})^2}{\Gamma_{\pm}^2}\right), \quad (6)$$

Here we denote Γ_{\pm} as the broadening of spin-up (+) and spin-down (-) Landau levels, respectively. To perform the simulations, the Fermi energy E_F is first calculated as a function of field from iterative solutions to the integral of the DoS multiplied by the Fermi distribution function in order to achieve the desired carrier density. The resistivity is obtained in the usual manner through inverting the conductivity tensor,

$$\rho_{xx} = \frac{\sigma_{xx}}{(\sigma_{xx}^2 + \sigma_{xy}^2)}, \quad (7)$$

where we use the classic expression for the Hall conductivity $\sigma_{xy} = -en_{2D}/B$ which is valid in low fields as done by previous authors.^{14,32} Γ_{\pm} is taken to be field independent.

To investigate the influence of broadening on the beating patterns, initially we set $\Gamma_+ = \Gamma_- = \Gamma$ and then simulate the magnetoresistance using narrow and large broadening parameters for a fixed spin splitting and carrier density. We used the parameters $n_{2D} = 3.3 \times 10^{15} \text{ m}^{-2}$, $\alpha_R = 1.3 \times 10^{-11} \text{ eVm}$, and $g^* = -30$. The resulting simulation using

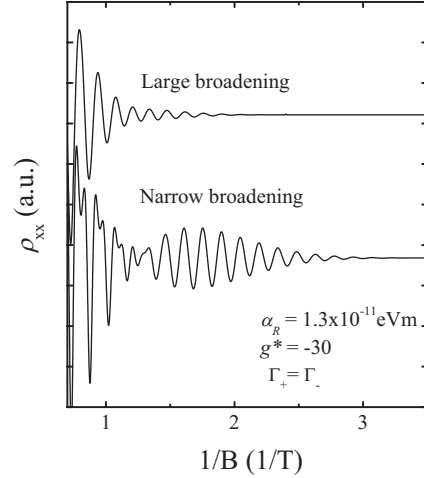


FIG. 7. Numerical simulations of ρ_{xx} for fixed spin splitting and carrier density with input parameters $\Gamma_+ = \Gamma_- = 1.6$ meV (lower trace) and $\Gamma_+ = \Gamma_- = 2.5$ meV (upper trace), demonstrating the disappearance of beating patterns at larger broadening.

$\Gamma = 1.6$ meV is shown in the lower trace in Fig. 7 and exhibits a pronounced beating pattern. In contrast, we see that the simulation with larger broadening, $\Gamma = 2.6$ meV, shown by the upper trace in Fig. 7, shows no discernible beating pattern consistent with the observations made in our experimental data.

This provides at least a semiquantitative basis for interpreting the absence of beating in the majority of our samples (although it is expected that the Rashba parameter will be smaller for lower carrier densities, further reducing the appearance of beating). We note also that in addition to the influence of broadening, competing spin splitting mechanisms which dominate in different regimes,¹⁸ i.e., the Dresselhaus splitting, may not be negligible at lower carrier densities and also influence the observed beating patterns. It is worth commenting that Brosig *et al.*³¹ also reported the absence of beating in high-quality InAs/AlSb and InAs/AlGaSb QWs over a range of carrier densities. In their samples, however, SdH oscillations were resolved at fields as low as $B \sim 150$ mT with a narrow broadening of $\Gamma \sim 0.4$ meV and so the absence of beating in their samples cannot be attributed to the same mechanism.

It is interesting that the numerical simulation of a narrow broadened sample (lower trace of Fig. 7) with the experimentally extracted Rashba parameter $\alpha_R \sim 1.3 \times 10^{-11} \text{ eVm}$ does not reproduce well our experimental data [shown in Fig. 5(a)] while good agreement has been found previously in the InGaAs system.¹⁴ The stronger beating pattern in the simulation suggests that the Rashba parameter used is larger than that in our samples. Furthermore, a zero amplitude beat node is not observed in the experimental data which is discussed below.

Spin-dependent scattering rates

The nonzero beat node amplitude in our data indicates that the SdH series originating from the two spin subbands oscillate at the Fermi energy with different amplitudes. This

conjecture is strongly supported by the unequal amplitudes of the spin-split peak in the FFT spectra (see the inset of Fig. 6). The observation of nonzero beat node amplitude was previously made by Lou *et al.*³² in a 10 nm InAs QW that was qualitatively interpreted by introducing the concept of a spin-dependent scattering process which suppresses the oscillation amplitude of one spin more than the other (although the nature of the mechanism is undetermined). This interpretation is based on the understanding that at low temperatures the SdH amplitude in the low-field region is predominantly determined by the single-particle relaxation time τ ,⁴⁶ which in remote doped structures is typically an order of magnitude smaller than the momentum scattering time.⁴⁷ Thus, in this interpretation there is a different scattering time τ_{\pm} associated with each spin. By varying the component of the magnetic field perpendicular to the sample in a tilted configuration (and hence the relative Zeeman splitting), Lou *et al.* demonstrated that the disparity between the two scattering times was proportional to the spin splitting in the system, be it from the SO interaction or external field. Thus the appearance of such features in our samples is consistent with the presence of a large spin splitting. Experimentally, τ can be extracted from the field dependence of the oscillation amplitude $\Delta\rho_{xx} \propto \exp(-\pi/\omega_c\tau)$ (Refs. 47 and 48); however, this is difficult when the two sets of oscillations are superimposed in the low-field region.

To explore this concept, we note that the broadening of the Landau levels is related to the single-particle relaxation rate by $\Gamma \propto \hbar\tau^{-\eta}$, where generally $\eta=1$ or $\eta=\frac{1}{2}$ dependent on the nature of the scattering.³³ The effects of spin-dependent scattering rates on the SdH oscillations can therefore be incorporated into the numerical simulations by introducing a spin-dependent level broadening into Eq. (6), i.e., $\Gamma_+ \neq \Gamma_-$. The result of this is demonstrated in Fig. 8(a) for the case where $\Gamma_+ > \Gamma_-$ with $\Gamma_+=1.6$ meV and $\Gamma_-=1.4$ meV (lower trace) compared to using equal broadening $\Gamma_+=\Gamma_-=1.6$ meV (upper trace). Here we have used a smaller Rashba parameter of $\alpha_R=9 \times 10^{-12}$ eV m to give closer resemblance to the experimental data. It can be seen that a spin-dependent broadening can indeed produce a nonzero beat node amplitude. The corresponding FFT spectra of the simulations with $\Gamma_+ > \Gamma_-$ and $\Gamma_+=\Gamma_-$ are shown in Fig. 8(b) by the solid and dotted lines, respectively. It can be seen that a spin-dependent broadening $\Gamma_+ > \Gamma_-$ also introduces an asymmetry in the spin-split FFT peak, consistent with that observed experimentally (see Fig. 5).

This provides compelling insight to the nature of the spin-dependent scattering in these samples. Based on these simulations we can determine that the majority (low energy) spin state is the spin-up state which undergoes greater scattering than the minority (high energy) spin-down state, i.e., $\tau_+^{-1} > \tau_-^{-1}$. The uniqueness of this interpretation is demonstrated by reversing the asymmetry of the input broadening parameters, i.e., $\Gamma_- > \Gamma_+$ with $\Gamma_+=1.4$ meV and $\Gamma_-=1.6$ meV. The resulting FFT spectrum from this simulation is shown in Fig. 8(c), which clearly exhibits the opposite peak asymmetry. From our analysis we cannot determine whether the spin-dependent scattering rates originate from a spin-dependent scattering mechanism or simply from the differing densities associated with each spin subband (related to a self-screening

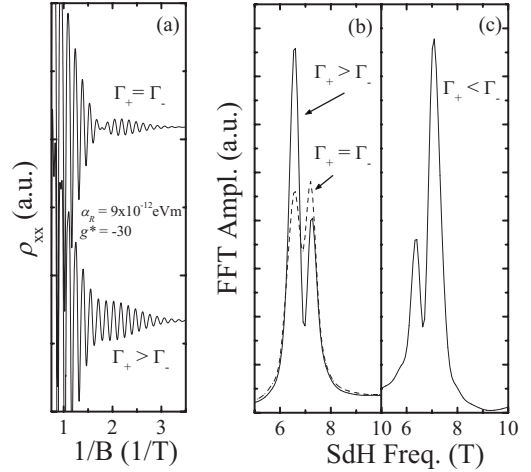


FIG. 8. (a) Simulations of ρ_{xx} with $\alpha_R=9 \times 10^{-12}$ eV m, $n_{2D}=3.3 \times 10^{15}$ m⁻², and $\Gamma_+=\Gamma_-=1.6$ meV (upper trace) compared to the results when using spin-dependent broadenings $\Gamma_+=1.6$ meV and $\Gamma_-=1.4$ meV. (b) FFT spectra of the simulations shown in (a) exhibiting asymmetric peak amplitudes when spin-dependent broadening is used (solid line) compared to the symmetric structure for the case of equal broadening for both spins (dashed line). (c) FFT spectrum of a simulation where the broadening parameters for each spin have been reversed exhibiting the opposite asymmetry in peak amplitude.

or even many-body effects). There are no intentional magnetic materials incorporated during the growth of our heterostructures which may preferentially scatter one spin orientation more than another. The assignment of the relative spin energies is expected for a system with a negative g factor. However, it is interesting to note that Lou *et al.* found the majority spin state to have the shorter scattering rate using a more indirect method.³² Although our observations and those of Ref. 32 differ, the samples studied in Ref. 32 are also structurally and electrically very different compared to ours, i.e., narrow QWs with high carrier densities and relatively low mobilities. Indeed, a more appropriate comparison would be to the work of Holmes *et al.* where a wide (30 nm) low-carrier-density InGaAs QW was studied¹⁵; the FFT data exhibited the same asymmetry as presented here (although no analysis of this feature was made in that paper). This suggests that both the structure and carrier density play a significant role in the relative spin scattering rates. Further study would be required in order to isolate any particular mechanism for this phenomenon and would benefit from measurements in tilted field.

IV. CONCLUSIONS

In summary we have presented high-field magnetotransport data from a range of high-mobility InSb QW samples as a function of temperature and gate bias. A detailed analysis of the level broadening in these samples was made indicating a clear relationship with the carrier density. Beating patterns were resolved in $d\rho_{xx}/dB$ and $d^2\rho_{xx}/dB^2$ only in samples with the narrowest broadening revealing a double-peaked structure in the FFT from which Rashba coupling parameters

were extracted. With the use of a top gate electrode we were able to demonstrate a small modulation in α_R over the range $1.3\text{--}1.5 \times 10^{-11}$ eV m. A clear signature of spin-dependent scattering was identified in the nonzero beat node amplitude and the asymmetric FFT of the data. Numerical simulations of the SdH oscillations demonstrated that both these features can be reproduced by using a spin-dependent broadening (hence scattering rate), strongly supporting the presence of such effects in these samples; a phenomenon shown to manifest in systems with large spin splitting. It is concluded that large Zeeman splitting alone cannot be responsible for the absence of beating in the majority of cases in these high-mobility samples but rather the combination of this with a

large and spin-dependent broadening. The majority (low energy) spin state is found to be the spin-up state, consistent with the presence of a negative g factor, which has a greater relaxation rate than the minority (high energy) spin-down state. The investigation of weak antilocalization in the extreme low-field limit is the subject of future work.

ACKNOWLEDGMENTS

This work was supported by the EPSRC under Grant No. EP/F065922. One of the authors (A.M.G.) wishes to thank J. J. Harris for helpful discussions during the course of this work.

-
- ¹G. Harbeke, O. Madelung, and U. Rossler, in *Functional Relationships in Science and Technology*, Landolt-Bornstein, New Series, Group III (Springer-Verlag, Berlin, 1982).
- ²T. Ashley, A. R. Barnes, L. Buckle, S. Datta, A. B. Dean, M. T. Emeny, M. Fearn, D. G. Hayes, K. P. Hilton, R. Jefferies, T. Martin, K. J. Nash, T. J. Phillips, W. H. A. Tang, and P. J. Wilding, Proceedings of the 7th International Conference on Solid-State and Integrated Circuits Technology, 2004, Vols. 1-3, p. 2253.
- ³S. A. Solin, D. R. Hines, A. C. H. Rowe, J. S. Tsai, Y. A. Pashkin, S. J. Chung, N. Goel, and M. B. Santos, Appl. Phys. Lett. **80**, 4012 (2002); S. A. Solin, D. R. Hines, J. S. Tsai, Y. A. Pashkin, S. J. Chung, N. Goel, and M. B. Santos, IEEE Trans. Magn. **38**, 89 (2002).
- ⁴K. L. Litvinenko, B. N. Murdin, J. Allam, C. R. Pidgeon, M. Bird, K. Morris, W. Branford, S. K. Clowes, L. F. Cohen, T. Ashley, and L. Buckle, New J. Phys. **8**, 49 (2006).
- ⁵X. Cartoixa, D. Z. Y. Ting, and Y. C. Chang, Appl. Phys. Lett. **83**, 1462 (2003); J. Schliemann, J. C. Egues, and D. Loss, Phys. Rev. Lett. **90**, 146801 (2003).
- ⁶S. Datta and B. Das, Appl. Phys. Lett. **56**, 665 (1990).
- ⁷S. Datta, T. Ashley, J. Brask, L. Buckle, M. Doczy, M. Emeny, D. Hayes, K. Hilton, R. Jefferies, T. Martin, T. J. Phillips, D. Wallis, P. Wilding, and R. Chau, in *Electron Devices Meeting, 2005, IEDM Technical Digest IEEE International*, 2005, p. 763.
- ⁸W. Knap, C. Skierbiszewski, A. Zduniak, E. Litwin-Staszewska, D. Bertho, F. Kobbi, J. L. Robert, G. E. Pikus, F. G. Pikus, S. V. Iordanskii, V. Mosser, K. Zekentes, and Y. B. Lyanda-Geller, Phys. Rev. B **53**, 3912 (1996).
- ⁹B. Das, D. C. Miller, S. Datta, R. Reifenberger, W. P. Hong, P. K. Bhattacharya, J. Singh, and M. Jaffe, Phys. Rev. B **39**, 1411 (1989).
- ¹⁰A. C. H. Rowe, J. Nehls, R. A. Stradling, and R. S. Ferguson, Phys. Rev. B **63**, 201307 (2001).
- ¹¹G. Engels, J. Lange, Th. Schäpers, and H. Lüth, Phys. Rev. B **55**, R1958 (1997).
- ¹²S. Ishida, K. Takeda, A. Okamoto, and I. Shibusaki, Physica E **20**, 211 (2004).
- ¹³J. Singleton, S. K. Greene, T. D. Golding, M. Pepper, C. Skierbiszewski, P. Wisniewski, P. J. Vanderwel, P. H. E. Vanthor, and J. Dinan, Superlattices Microstruct. **9**, 51 (1991).
- ¹⁴J. Nitta, T. Akazaki, H. Takayanagi, and T. Enoki, Phys. Rev. Lett. **78**, 1335 (1997).
- ¹⁵S. N. Holmes, P. J. Simmonds, H. E. Beere, F. Sfigakis, I. Farrer, D. A. Ritchie, and M. Pepper, J. Phys.: Condens. Matter **20**, 472207 (2008).
- ¹⁶A. R. Dedigama, D. Jayathilaka, S. H. Gunawardana, S. Q. Murphy, M. Edirisooriya, N. Goel, T. D. Mishima, and M. B. Santos, *Narrow Gap Semiconductors 2007*, Springer Proceedings in Physics, Vol 119, p. 35 (2008).
- ¹⁷G. A. Khodaparast, R. E. Doezema, S. J. Chung, K. J. Goldammer, and M. B. Santos, Phys. Rev. B **70**, 155322 (2004).
- ¹⁸A. M. Gilbertson, M. Fearn, J. H. Jefferson, B. N. Murdin, P. D. Buckle, and L. F. Cohen, Phys. Rev. B **77**, 165335 (2008).
- ¹⁹M. Akabori, V. A. Guzenko, T. Sato, T. Schaepers, T. Suzuki, and S. Yamada, Phys. Rev. B **77**, 205320 (2008).
- ²⁰J. M. S. Orr, A. M. Gilbertson, M. Fearn, O. W. Croad, C. J. Storey, L. Buckle, M. T. Emeny, P. D. Buckle, and T. Ashley, Phys. Rev. B **77**, 165334 (2008).
- ²¹W. R. Branford, A. M. Gilbertson, P. D. Buckle, L. Buckle, T. Ashley, F. Magnus, S. K. Clowes, J. J. Harris, and L. F. Cohen, *Narrow Gap Semiconductors* **119**, 3 (2008).
- ²²W. Schneider, H. Bruhns, and K. Hubner, J. Phys. Chem. Solids **41**, 313 (1980).
- ²³E. S. Kannan, G. H. Kim, S. Kumar, I. Farrer, D. A. Ritchie, J. H. Son, J. M. Baik, J. L. Lee, D. H. Youn, and K. Y. Kang, Appl. Phys. Lett. **90**, 152110 (2007).
- ²⁴R. J. Nicholas (private communication).
- ²⁵P. A. Lee and T. V. Ramakrishnan, Rev. Mod. Phys. **57**, 287 (1985).
- ²⁶W. R. Branford, A. Husmann, S. A. Solin, S. K. Clowes, T. Zhang, Y. V. Bugoslavsky, and L. F. Cohen, Appl. Phys. Lett. **86**, 202116 (2005).
- ²⁷E. Kane, in *Narrow Gap Semiconductors Physics and Applications*, edited by W. Zawadzki (Springer-Verlag, Berlin, 1980), Vol. 133, pp. 13; P. Pfeffer and W. Zawadzki, Phys. Rev. B **41**, 1561 (1990).
- ²⁸W. Zawadzki, Adv. Phys. **23**, 435 (1974).
- ²⁹B. Nedninyom, R. J. Nicholas, M. Emeny, L. Buckle, A. M. Gilbertson, P. D. Buckle, and T. Ashley, Phys. Rev. B (to be published).
- ³⁰R. J. Nicholas, R. J. Haug, K. Vonklitzing, and G. Weimann, Phys. Rev. B **37**, 1294 (1988).
- ³¹S. Brosig, K. Ensslin, R. J. Warburton, C. Nguyen, B. Brar, M.

- Thomas, and H. Kroemer, Phys. Rev. B **60**, R13989 (1999).
- ³²J. Luo, H. Munekata, F. F. Fang, and P. J. Stiles, Phys. Rev. B **41**, 7685 (1990).
- ³³T. Ando, A. B. Fowler, and F. Stern, Rev. Mod. Phys. **54**, 437 (1982).
- ³⁴J. P. Heida, B. J. van Wees, J. J. Kuipers, T. M. Klapwijk, and G. Borghs, Phys. Rev. B **57**, 11911 (1998).
- ³⁵D. Grundler, Phys. Rev. Lett. **84**, 6074 (2000).
- ³⁶V. A. Guzenko, T. Schapers, and H. Hardtdegen, Phys. Rev. B **76**, 165301 (2007).
- ³⁷T. Schapers, G. Engels, J. Lange, T. Klocke, M. Hollfelder, and H. Luth, J. Appl. Phys. **83**, 4324 (1998).
- ³⁸Y. A. Bychkov and E. I. Rashba, J. Phys. C **17**, 6039 (1984).
- ³⁹C. M. Hu, J. Nitta, T. Akazaki, H. Takayanagai, J. Osaka, P. Pfeffer, and W. Zawadzki, Phys. Rev. B **60**, 7736 (1999).
- ⁴⁰P. Pfeffer and W. Zawadzki, Phys. Rev. B **59**, R5312 (1999).
- ⁴¹E. A. de Andrada e Silva, G. C. La Rocca, and F. Bassani, Phys. Rev. B **55**, 16293 (1997).
- ⁴²C. H. Yang, W. Xu, J. Zhang, Z. Zeng, and C. Zhang, Physica E **40**, 1979 (2008).
- ⁴³P. Pfeffer and W. Zawadzki, Phys. Rev. B **68**, 035315 (2003).
- ⁴⁴R. Winkler, *Spin-Orbit Coupling Effects in Two-Dimensional Electron and Hole Systems* (Springer-Verlag, Berlin, 2003), Vol. 191, p. 1.
- ⁴⁵R. R. Gerhardts, Z. Phys. B **21**, 285 (1975).
- ⁴⁶P. T. Coleridge, R. Stoner, and R. Fletcher, Phys. Rev. B **39**, 1120 (1989).
- ⁴⁷P. T. Coleridge, Phys. Rev. B **44**, 3793 (1991).
- ⁴⁸U. Bockelmann, G. Abstreiter, G. Weimann, and W. Schlapp, Phys. Rev. B **41**, 7864 (1990).